DISLOCATION EMISSION AT FIBERS—I. THEORY OF LONGITUDINAL PUNCHING BY THERMAL STRESSES

D. C. DUNAND and A. MORTENSEN

Department of Materials Science and Engineering, Massachusetts Institute of Technology,
Cambridge, MA 02139, U.S.A.

Abstract—A model predicting the number of prismatic loops dislocation punched at the ends of a cylindrical fiber by thermal mismatch stresses is presented. The longitudinal stress in the fiber is derived as a function of the distance from fiber center using the shear-lag model for the elastic portion of the interface. We show that there is a critical fiber length above which the number of loops is constant. This is because the central part of the fiber is strained by plastic and elastic interfacial shear until it exhibits no mismatch with the matrix. The backstress of the loops on the fiber is derived and the effect of the fiber stress field on the loops is estimated away from the corner singularity. The analysis allows prediction of both the punching distance and the dislocation density in the row of loops. Finally, a parametric study is performed on the system Al/Al$_2$O$_3$ and the results are compared to an existing and different model.

Résumé—On présente un modèle prévoyant le nombre de boucles prismatiques de dislocations produites aux extrêmités d'une fibre cylindrique par les contraintes de désaccord thermique. La contrainte longitudinale dans la fibre est calculée en fonction de la distance du centre de la fibre en utilisant le modèle de retard au cisaillement pour la portion élastique de l'interface. Nous montrons qu'il existe une longueur critique de fibre au dessus de laquelle le nombre de boucles est constant. Ceci est lié au fait que la partie centrale de la fibre est déformée par un cisaillement interfacial plastique et élastique jusqu'à ce qu'elle ne présente aucun désaccord avec la matrice. Les contraintes en retour des boucles sur la fibre sont calculées et l'effet du champ de contrainte de la fibre sur les boucles est estimé loin de la singularité de coin. L'analyse permet de prévoir à la fois la distance d'interaction et la densité de dislocations dans la rangée de boucles. Enfin, une étude paramétrique est effectuée sur le système Al/Al$_2$O$_3$ et les résultats sont comparés à un modèle différent.

Zusammenfassung—Es wird ein Modell vorgelegt, welches das Ausstoßen prismatischer Versetzungsschleifen an den Enden zylindrischer Fasern durch thermische Fehlpassungsspannungen beschreibt. Die longitudinale Spannung in den Fasern wird in Abhängigkeit vom Abstand von der Fasermitte abgeleitet, idem ein Scherverzögerungsmodell für den elastischen Teil der Grenzfläche benutzt wird. Wir zeigen, daß eine kristische Faserlänge besteht, oberhalb der die Zahl der Versetzungsschleifen konstant ist. Diese Tatsache rührt daher, daß der zentrale Teil der Faser durch plastische und elastische Grenzflächenscherung verformt wird, bis keine Fehlpassung zur Matrix mehr besteht. Die Rückspannung der Versetzungsschleifen auf die Faser wird abgeleitet; der Einfluß des Spannungsfeldes der Faser auf die Versetzungsschleifen wird für Bereiche außerhalb der EckSingularität abgeschätzt. Die Analyse ermöglicht, sowohl Ausstoßabstand wie auch die Versetzungsdichte in der Reihe der Versetzungsschleifen vorauszusagen. Schließlich wird das System Al/Al$_2$O$_3$ parametrisch studiert; die Ergebnisse werden mit einem vorhandenen, aber sich unterscheidendem Modell verglichen.

1. INTRODUCTION

When a two-phase material is subjected to a temperature change, internal stresses are generated if the two constituents have different Coefficients of Thermal Expansion (CTEs). If one of the phases (usually the matrix) deforms by slip, plastic relaxation can occur, thus retarding or suppressing fracture of the matrix, reinforcement or interface. Prismatic loop punching due to thermal stresses has been observed in metals with submicroscopic particles of spherical [1] and irregular [2, 3] shape, salts containing large spheres [4, 5], particles [6] or fibers [5, 7], as well as metal matrix composites reinforced with large particles [8] and whiskers [9, 10].

A theoretical understanding of thermally induced plasticity in metal matrix composites is important since dislocations produced during thermal cycling or cooling from manufacturing temperature can influence such properties as yield stress, strain-hardening, residual stresses, creep and dimensional stability of the composite. While many models exist which consider the elastic stresses around fibers, only one—to the best of our knowledge—proposed by Taya and Mori [10] and later used by Christman and Suresh [11], describes loop punching at the end of the fibers. This model, briefly summarized in Appendix B, approximates fibers with spheroids and uses Eshelby's equivalent inclusion model [12] assuming a continuous distribution of dislocations to predict the punching distance by the spheroids.

The model presented in this article is an attempt to treat the problem of thermally induced prismatic loops punched longitudinally by cylindrical fibers, using the shear-lag approximation by Cox [13] and dislocation theory. We first derive the number of loops in the elasto-plastic case and give expressions for the fiber stress, the interfacial shear stress and the backstress due to the punched dislocations. We then determine the punching distance using existing expressions for the equilibrium of a row of loops and by estimating the effect on the loops of the fiber residual stresses. We finally perform a parametric study on the system Al/Al$_2$O$_3$ to illustrate the model described above and compare it to that of Ref. [10].

2. THEORY

Consider a perfectly elastic fiber in a matrix capable of plastic deformation by dislocation movement. Upon cooling from an elevated temperature, thermal stresses will develop due to the CTE mismatch between the fiber and the matrix. We neglect the radial stresses, which are small compared to the axial stresses for a slender body, and we assume an elastic, perfectly plastic matrix showing no strain-hardening. At high temperature, the fiber is embedded in the matrix and both phases are initially stress-free. Upon cooling, the matrix shrinks more than the fiber if we assume that the matrix CTE is larger than that of the fiber (as is the case in most metal matrix composite systems). This results in a stressed interface with the fiber in compression and the matrix in tension. At first, the interface is stressed elastically by shear along the whole length of the fiber. As the temperature decreases, the total mismatch strain between fiber and matrix increases and the interfacial shear stress increases proportionally. At some temperature, function of the fiber length, the interfacial shear stress may equal the matrix plastic flow stress, at which point dislocation motion is induced in the matrix. This changes the nature of the stress distribution along the fiber, just as it does in a short fiber composite in tension [14]. Whatever the nature of the stress at the interface, so long as there is no debonding (a situation which we exclude here), stress builds up in the fiber as the result of load transfer from the matrix. The resulting fiber strain reduces the local mismatch between fiber and matrix.

In summary, three different local situations are possible at the fiber–matrix interface, which may occur simultaneously or separately along the same fiber:

—unstrained interface: the fiber is stressed elastically to a strain equal to the CTE mismatch strain;
—elastic interface: both fiber and matrix are stressed elastically; the interfacial shear stress is everywhere lower than the critical shear stress at which slip is initiated;

—plastic interface: the critical shear stress is reached, thus inducing slip at the interface.

2.1. Elastic regime

Consider a cylindrical fiber of length L, diameter d, parallel to the x-axis and centered at the origin. We use a shear lag model developed by Cox [13] for a single fiber embedded in a matrix submitted to an uniaxial strain e at infinity applied along the same direction as the main axis of the fiber. In this model, it is assumed that

$$\frac{dp}{dx} = H''(u - w) \tag{1}$$

where p is the load on the fiber, H'' is a constant, u is the longitudinal displacement in the fiber and w is the hypothetical displacement at the same point in the absence of the fiber. The axial stress in the fiber $\sigma(x)$ can then be expressed as

$$\sigma(x) = E_f \cdot e \left[1 - \frac{\cosh(\beta \cdot x)}{\cosh(\beta \cdot L/2)} \right] \tag{2}$$

and the interfacial shear stress $\tau(x)$ is

$$\tau(x) = \frac{E_f \cdot d \cdot e \cdot \beta}{4 \cdot \cosh(\beta \cdot L/2)} \sinh(\beta \cdot x) \tag{3}$$

where

$$\beta = \left[\frac{8 \cdot G_m}{E_f \cdot d^2 \cdot \ln(v_f^{-1/2})} \right]^{1/2} \tag{4}$$

and E_f is the fiber elastic modulus, x the distance from the origin, G_m the matrix shear modulus and v_f the fiber volume fraction. Equations (2) and (3) are connected by

$$\frac{d\sigma(x)}{dx} = -\frac{4}{d} \cdot \tau(x). \tag{5}$$

This analysis, which was later refined by Dow [15], was found to be experimentally correct by Schuster and Scala [16] as well as Tyson and Davies [17], except close to the ends of the fibers (about two diameters from the extremity) where the measured shear stress was higher than predicted by Cox [13] due to the stress concentration at the end faces discontinuity. Figure 1(a) shows schematically the interfacial shear stress which is zero at the fiber center and maximum at its ends. Since the fiber longitudinal stress is built up from the shear stress transfer from the matrix, it is zero at fiber ends (assuming no load transfer from the end faces) and maximum at the fiber center.

We assume that equation (1) is valid for the case where the matrix shrinks (or expands) around a fiber, neglecting the radial strains. The same equations used for the shear-lag model [equations (1)–(4)] can then be used if the external strain e is assimilated to the thermal mismatch strain

$$e = \Delta\alpha \cdot \Delta T \tag{6}$$
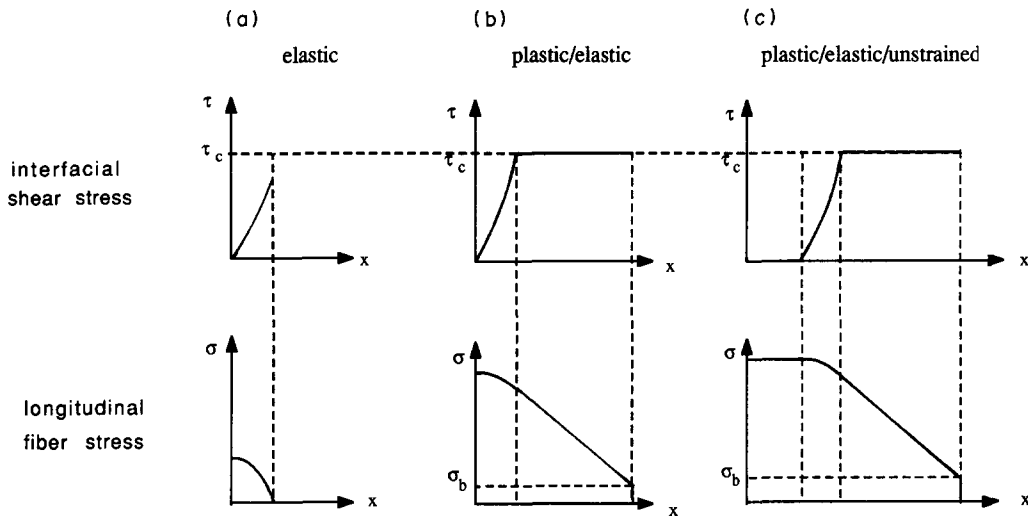
with

$$\Delta\alpha = \alpha_m - \alpha_f \tag{7}$$

(a)   (b)   (c)
elastic   plastic/elastic   plastic/elastic/unstrained

Fig. 1. (a–c) Schematic diagrams for the interfacial shear stress τ and the fiber longitudinal stress σ as a function of the distance x from the center of the fiber. (a) Purely elastic interface, (b) plastic–elastic interface, (c) plastic–elastic–unstrained interface.

where α_m and α_f are respectively the matrix and fiber coefficient of thermal expansion and ΔT is the temperature difference between the higher temperature (stress-free state) and the lower temperature (stressed state). The axial fiber stress and the interfacial shear stress are found by inserting equation (6) into equations (2) and (3).

As can be seen from equation (2), the fiber longitudinal stress increases as x decreases and is maximum at the fiber center. Simple inspection of equation (2), however, shows that the maximum fiber stress (at $x = 0$) will never reach the value $E_f e$ for a fiber of finite length L. Thus, in the purely elastic case, an unstrained interface cannot occur under the present assumptions, except of course at the exact center of the fiber.

The interfacial shear stress is maximum at the fiber end ($x = L/2$) and increases as L increases. At some critical fiber length L_p. the critical shear stress τ_c is reached at the end of the fiber where plastic flow and dislocation emission begin. Introducing equation (6) as well as the values

$$\tau = \tau_c \tag{8a}$$

$$x = L_p/2 \tag{8b}$$

$$L = L_p \tag{8c}$$

in equation (3) gives an equation for L_p

$$L_p = \frac{2}{\beta} \text{arctgh} \left[\frac{4 \cdot \tau_c}{\beta \cdot E_f \cdot d \cdot \Delta\alpha \cdot \Delta T} \right]. \tag{9}$$

If the fiber is longer than L_p, the interface at the ends of the fiber is plastic. We now consider the case when this happens.

2.2. Plastic–elastic regime

In the unstrained state at a higher temperature, the fiber of length L_0 can be thought of as occupying a hole of same length in the matrix [Fig. 2(a)]. Upon

cooling by a temperature interval of ΔT, the fiber length —if it were outside the matrix—would become L_f while the hole in the matrix in absence of the fiber would have a length L_m. Fitting the fiber in the hole will force both the fiber and the hole to adopt a length L, which is intermediate between L_f and L_m [Fig. 2(b)].

It is assumed that slip is the only relaxation mechanism in the temperature interval ΔT, and that the fiber axis is oriented along a slip direction. Plasticity originates from the fiber end because the shear stress is maximum there and because the fiber end corner acts as a stress concentrator. The end of the fiber then acts like a punch and creates a pair of prismatic dislocation loops with opposite Burgers vector parallel to the fiber axis. One of these is a prismatic interstitial loop which glides away from the fiber end into the matrix, repelled by the local stress field of the fiber and that of subsequently formed interstitial loops. The vacancy loop can be thought as gliding in the other direction along the interface away from the fiber end and relaxing the stressed interface. The glide length defines the plastic zone. In reality, it is more probable that the vacancy loops are delocalized along the whole length of the plastic zone, i.e. the atomic planes shift slightly due to the addition of an additional plane at the interface, leading to a reduction of the elastic stress at the fiber end. The plastic zone can be thought of as the interfacial length where this shift is appreciable. The fiber thus relaxes its interface and emits in the matrix along the x-axis a row of coaxial, circular, interstitial, prismatic dislocation loops of diameter d. Since each loop carries away a disk of matrix material of thickness equal to its Burgers vector b, the number of loops n punched at each end is, by conservation of volume

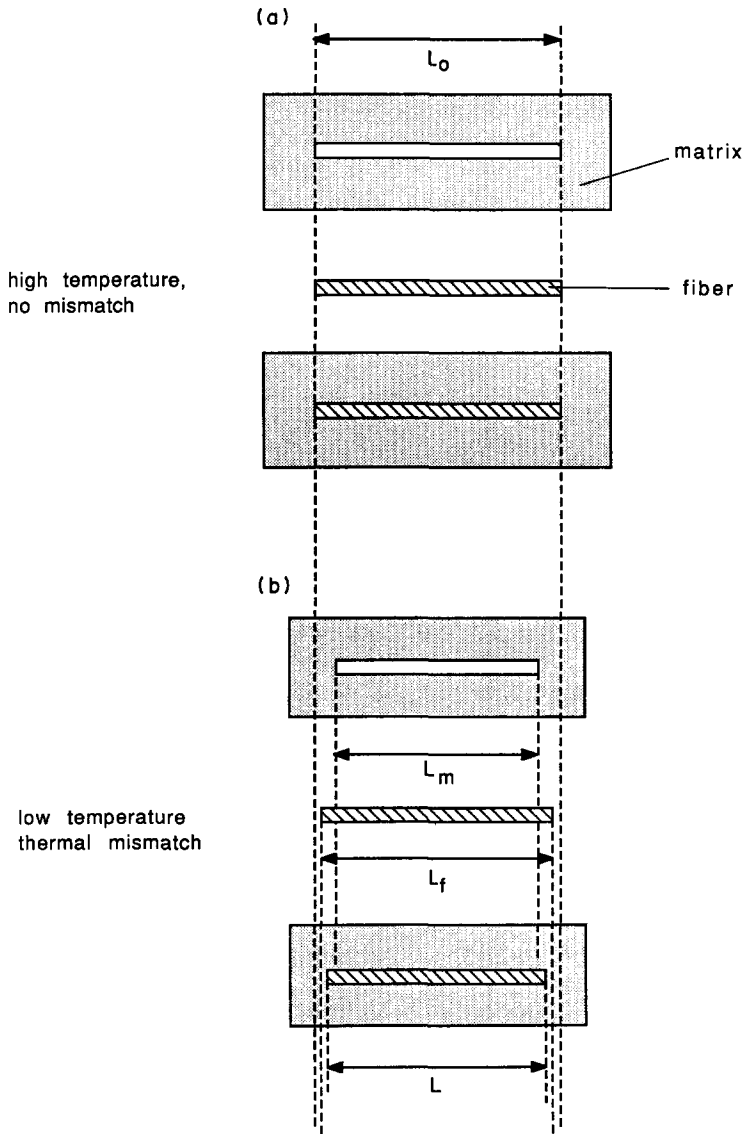$$n = \frac{L - L_m}{2 \cdot b}. \tag{10}$$

Fig. 2. (a, b) Schematic diagram of matrix, fiber and composite before (a) and after (b) the temperature change ΔT.

Now, Hooke's law applied to the elastic fiber gives

$$\frac{L_f - L}{L} = \frac{\bar{\sigma}}{E_f} \qquad (11)$$

where the average stress in the fiber is

$$\bar{\sigma}(L) = \frac{2}{L} \cdot \int_0^{L/2} \sigma(x) \, dx \qquad (12)$$

while the CTE equations yield

$$\frac{L_0 - L_m}{L_m} = \alpha_m \cdot \Delta T \qquad (13)$$

$$\frac{L_0 - L_f}{L_f} = \alpha_f \cdot \Delta T \qquad (14)$$

assuming isotropic and temperature independent CTEs. Combining equations (7), (10), (11), (13) and (14) then gives

$$n = \frac{L}{2 \cdot b \cdot (1 + \alpha_m \cdot \Delta T)}$$

$$\times \left[\Delta \alpha \cdot \Delta T - (1 + \alpha_f \cdot \Delta T) \cdot \frac{\bar{\sigma}}{E_f} \right]. \qquad (15)$$

Thus, one only needs to evaluate the average stress $\bar{\sigma}(L)$ defined in equation (12) to find through equation (15) the number of loops punched at the end of the fiber. This necessitates a knowledge of the function $\sigma(x)$ or equivalently of $\tau(x)$ [equation (5)].

The fiber longitudinal stress is shown schematically in Fig. 3. The integral of this stress function can
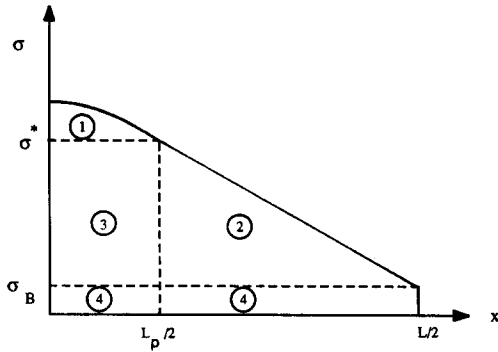
Fig. 3. Diagram for the longitudinal stress for a fiber of length L in the plastic–elastic regime.

be decomposed in four parts [right-hand side of equation (16)] labelled 1 to 4 in Fig. 3

$$\bar{\sigma}(L) = \frac{2}{L} \cdot \int_0^{L_p/2} \sigma_e(x)\,dx + \frac{(\sigma^* - \sigma_B)}{2 \cdot L} \cdot (L - L_p)$$

$$+ \frac{(\sigma^* - \sigma_B)}{L} \cdot L_p + \sigma_B \quad (16)$$

where σ^* is the fiber longitudinal stress at the point where the interfacial shear stress reaches its critical value τ_c, σ_B is the backstress on the end face of the fiber by the punched loops and $\sigma_e(x)$ is the contribution by the elastic interface to the fiber longitudinal stress. In what follows, we determine these three variables.

We first evalute the integral of $\sigma_e(x)$. The elastic stress profile $\sigma_e(x)$ is independent of the fiber total length in the elastic–plastic regime. In other words, the stress diagrams of fibers of different lengths in that regime will match when superimposed. Figure 4(a) shows the superimposed diagrams of the interstitial shear stress for three fibers of length L_p, L and L_u such that $L_p \leqslant L \leqslant L_u$, the length L_u corresponding to the boundary between the elastic–plastic and the elastic–plastic-unstrained regimes. It follows from equation (5) that the fiber longitudinal stress diagrams can also be superimposed, with a shift of the coordinate system due to the integration variable. This is shown schematically in Fig. 4(b–d) for the same three fiber lengths as in Fig. 4(a) (the backstress σ_B increases with the length of the fiber and is derived in Appendix A). The first term of the right hand side of equation (16) is thus independent of the fiber length and can be calculated by integrating equation (2) with $L = L_p$. This yields after introduction of equations (6) and (9)

$$\frac{2}{L} \cdot \int_0^{L_p/2} \sigma_e(x)\,dx = E_f \cdot \Delta\alpha \cdot \Delta T \cdot \frac{L_p}{L} - \frac{8 \cdot \tau_c}{\beta^2 \cdot d \cdot L}. \quad (17)$$

We now determine σ^*, the stress induced in the fiber by the plastic interfacial region. Considering the fiber of length $L > L_p$, the interfacial shear stress and fiber stress gradient in the plastic interface

region, i.e. for values of x between $L_p/2$ and $L/2$ are respectively [Fig. 4(c)]

$$\tau(x) = \tau_c, \quad (18)$$

$$\frac{d\sigma(x)}{dx} = 2 \cdot \frac{\sigma^* - \sigma_B}{L - L_p}. \quad (19)$$

Inserting equations (18) and (19) into equation (5) then gives an expression for σ^*

$$\sigma^* = \frac{2 \cdot \tau_c}{d}(L - L_p) + \sigma_B. \quad (20)$$

Inserting equations (17) and (20) into (16) finally yields

$$\bar{\sigma}(L) = E_f \cdot \Delta\alpha \cdot \Delta T \cdot \frac{L_p}{L}$$

$$+ \frac{\tau_c}{d \cdot L}(L^2 - L_p^2 - 8 \cdot \beta^{-2}) + \sigma_B \quad (21)$$

where σ_B is given in Appendix A, equation (A1).

Inserting equations (21) and (A1) into equation (15) gives an equation for the total number of loops n as a function of geometrical and thermomechanical
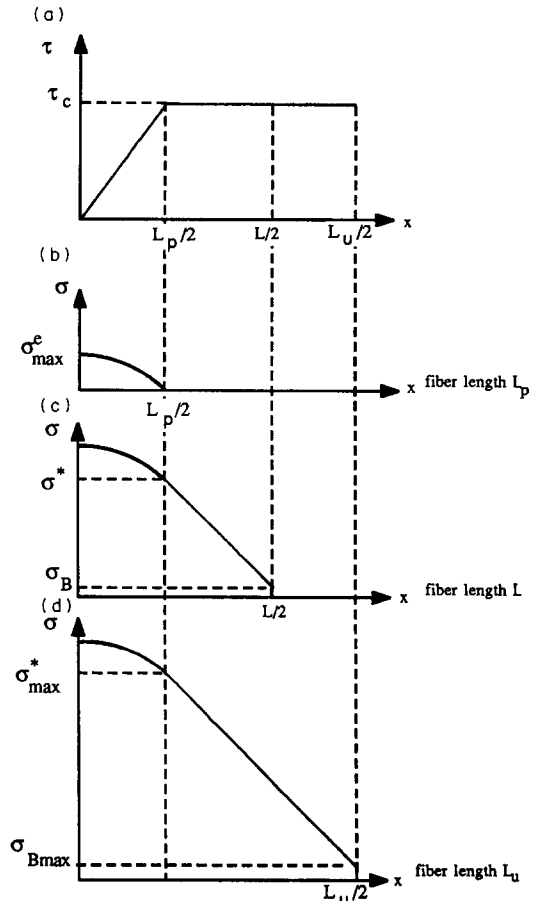

Fig. 4. (a–d) Superimposed diagrams for the interfacial shear stress (a) and the corresponding diagrams for the fiber longitudinal stress (b–d) for three different fiber lengths L_p, L, L_u.

parameters, all assumed to be isotropic and temperature independent

$$n = \left(1 + \frac{(1 + \alpha_f \Delta T) \cdot 2 \cdot L \cdot \tau_c}{(1 + \alpha_m \Delta T) \cdot d \cdot E_f} \right)^{-1} n' \qquad (22)$$

where

$$n' = \frac{L}{2 \cdot b \cdot (1 + \alpha_m \Delta T)}$$

$$\times \left\{ \frac{\tau_c}{d \cdot E_f} (1 + \alpha_f \Delta T) \left(L_p^2 + \frac{8}{\beta^2} - L^2 \right) \right.$$

$$\left. + \Delta \alpha \cdot \Delta T \cdot [L - L_p \cdot (1 + \alpha_f \Delta T)] \right\} \qquad (23)$$

is the solution of equation (21) for $\sigma_B = 0$. For most systems of interest, σ_B is very small and thus n and n' are almost equal.

2.3. Plastic–elastic–unstrained regime

In the elastic–plastic regime, the maximum fiber stress in the central fiber region increases with increasing fiber length since the length of the plastic region increases too, loading the fiber linearly from the fiber ends [equations (5) and (18)]. Above a certain critical length L_u, the fiber will be strained by the matrix to such a degree that a region in the middle of the fiber forms, devoid of strain mismatch with the matrix. The interfacial displacement and shear stress are zero in that region, and the fiber strain has a value of $\Delta \alpha \Delta T$.

L_u is the critical length of the fiber between the two regimes plastic–elastic and plastic–elastic–unstrained, corresponding to the fiber length where the maximum strain $\Delta \alpha \Delta T$ is just reached at the center of the fiber. The interfacial shear stress and fiber stress are shown in Fig. 4(d). The fiber stress at the origin is maximum and has the value

$$\sigma(0) = E_f \cdot \Delta \alpha \cdot \Delta T. \qquad (24)$$

From Fig. 4(b) and 4(e), we find

$$\sigma(0) = \sigma_{e,max} + \sigma_{max}^* \qquad (25)$$

where $\sigma_{e,max}$ and σ_{max}^* are the stress contributions from the elastic and plastic interface regions respectively. Inserting equation (2) (with $x = 0$ and $L = L_p$), equation (20) (with $L = L_u$ and $\sigma_B = \sigma_{Bmax}$) and equation (24) into equation (25) yields

$$L_u = L_p + \frac{E_f \cdot d \cdot \Delta \alpha \cdot \Delta T}{2 \cdot \tau_c \cdot \cosh(\beta \cdot L_p/2)} - d \cdot \frac{\sigma_{Bmax}}{2 \cdot \tau_c} \qquad (26)$$

where σ_{Bmax} is the backstress on the fiber of length L_u.

Inserting $L = L_u$ as given by equation (26) into equations (22) or (23) gives the maximum number of punched loops. Any fiber of length larger than L_u will punch this maximum number of loops regardless of its length, since the unstrained length

in its center part does not contribute to the strain mismatch.

In summary, depending upon the length of the fiber and the values of the thermomechanical properties of the fiber and the matrix, three main global regimes can be distinguished for a given fiber:

(a) Elastic regime: the whole interface is elastic; the interfacial shear stress is everywhere below the interfacial critical shear stress and no dislocation loops are created.

(b) Plastic–elastic regime: both ends of the fiber have a plastic interface while the interface away from the end is elastic. The plastic interface forms when the fiber tip creates pairs of prismatic loops of vacancy and interstitial character respectively. The interstitial loop is punched from the fiber end into the matrix and glides away from the fiber. It leaves behind a vacancy loops which glides in the opposite direction along the fiber interface to relieve the interfacial mismatch.

(c) Plastic–elastic–unstrained regime: the interface at both ends of the fiber is stressed plastically and then elastically; the load transfer is such that the central part of the fiber is elastically strained to the point that there is no local mismatch with the matrix, leading to an unstrained interface.

Figure 1(a–c) schematically show the interfacial shear stress and fiber axial stress for the three cases cited above; only half of the fiber is represented since these functions are symmetric with respect to the origin. We note that an elastic zone always exists because the interfacial displacement and thus the shear stress are zero at the fiber center.

2.4. Punching distance

The number of loops punched by a fiber was derived in the previous paragraph. From this information, it is possible to determine the length of plastic zone formed by the row of punched loops by equilibrating the system of loops in the matrix. Since all loops of identical Burgers vector repel each other, each loop is subjected to a stress pushing it away from the fiber by its neighbors closer to the fibers, and toward the fiber by its neighbors farther away from it. Each loop (except the one closest to the fiber) will move away from the fiber on its glide cylinder until it is subjected to a shear stress in the positive x direction equal to the lattice friction stress. This is true for the loop closest to the fiber as well if the residual elastic stress of the fiber is sufficient to counteract the stress of all the other loops. Alternatively, if the contribution of the other loops is large enough, this first loop will be pushed against the interface and prevented from moving farther. In either case, the loop closest to the fiber can be thought of as blocked, while all other loops are free to glide in the positive x direction, but prevented from moving an infinite distance by the lattice friction stress τ_f.

In a recent paper [18], we computed the row length for different values of the total number of loops n and of the dimensionless parameter v

$$v = \frac{2 \cdot \pi \cdot d \cdot (1 - v) \cdot \tau_f}{b \cdot G} \qquad (27)$$

where G and v are the matrix shear modulus and Poisson's ratio and b is the loop Burgers vector. We took into account all neighbors excerting a stress larger than the friction stress and found that, for $25 \leqslant n \leqslant 400$ and $0.05 \leqslant v \leqslant 5$, the row length L_r can be fitted to

$$L_r = 1.74 \cdot d \cdot v^{-0.64} \cdot n^{0.34}. \qquad (28)$$

Equations (22) and (23) can be inserted into equation (28) to yield the row length, calculated from the first loop. The length of the plastic zone is found by adding the distance between the loop closest to the fiber and the fiber end. As shown in the next paragraph, this length is small and is therefore neglected in the calculation of the punching distance which is taken as L_r. The average dislocation density ρ in the volume defined by the glide cylinder and the first and last loop is then

$$\rho = \frac{4 \cdot n}{d \cdot L_r} \qquad (29)$$

or, introducing equation (28) into equation (29)

$$\rho = \frac{2.30 \cdot v^{0.64} \cdot n^{0.66}}{d^2}. \qquad (30)$$

Due to the unequal spacing of the loops, this density is not constant in the glide cylinder, being higher than average close to the fiber and lower at the other end of the row.

2.5. Effect of fiber residual stresses on punching distance

In what follows, we estimate the shear stress in the vicinity of a fiber with residual stresses and its effect on the punching distance. Even after punching, the fiber and the interface are stressed elastically as shown in the previous paragraphs, thus inducing a shear stress on the glide cylinder which can alter the equilibrium position of the row of loops and therefore the row length [equation (28)]. We showed in a recent article [18] that large perturbations in the stress state at the row end closest to the blocked loop do not significantly change the row length. On the other hand, perturbations at the "free" end of the row have much larger effects on the local loop spacings and thus the row length.

We do not seek to evaluate the stress close to the sharp corner formed by the end of the cylinder. It is likely to be high in the immediate vicinity of the singularity and to decay rapidly away from it. For instance, Schneider and Conway [19] found that, at a distance of 0.14 diameter from the end of a flat-end rectangular fiber, the shear stress was only a third of the uniform tensile stress applied at infinity. Similarly, Atkinson et al. [20] found that the shear stress decays very rapidly in the matrix close to the end of a partially embedded fiber subjected to a pull-out test. Except in the small region close to the stress singularity, the matrix stress is dominated by the contribution of the residual fiber stress; this matrix shear stress is calculated in what follows on the glide cylinder where the loops are located.

Let us represent the fiber by a semi-infinite cylinder of diameter d, the end of which is at the origin of a cylindrical coordinate system z, r, θ. It is assumed that the interfacial shear stress along the fiber is constant and equal to its maximal value τ_c, corresponding to a fully plastic interface. These two assumptions, of semi-infinite fiber and fully plastic interface, will yield an upper bound for the matrix shear stress since actual fibers are finite in length and since the interfacial shear strength can only be constant up to the middle of the fiber where its sign is reversed. Following Phan–Thien [21], the fiber is considered as a slender body which can be approximated by a suitable distribution of "Kelvinlets" or point forces. For the conditions stated above, the relevant Kelvinlets are

$$dF_z = -\pi \cdot d \cdot \tau_c \cdot dz, \qquad (31)$$

$$dF_r = 0, \qquad (32)$$

$$dF_\theta = 0. \qquad (33)$$

Landau and Lifshitz [22] give the displacement field **u** at a point **x** due to a force **F** applied at the origin of a cartesian coordinate system x_1, x_2, x_3 as

$$du_i(x) = \frac{1}{16 \cdot \pi \cdot G \cdot (1 - v)}$$

$$\times \left[\frac{3 - 4v}{(x_1^2 + x_2^2 + x_3^2)^{1/2}} \delta_{ij} \right.$$

$$\left. + \frac{x_i \cdot x_j}{(x_1^2 + x_2^2 + x_3^2)^{3/2}} \right] \cdot dF_j \qquad (34)$$

where δ_{ij} is the Kronecker symbol, G the matrix shear modulus and v its Poisson's ratio. Introducing equations (31)–(33) into equation (34) and using cylindrical coordinates yields

$$du_z = -\frac{d \cdot \tau_c}{16 \cdot G \cdot (1 - v)} \cdot \frac{r \cdot z}{(r^2 + z^2)^{3/2}} dz, \qquad (35)$$

$$du_r = \frac{d \cdot \tau_c}{16 \cdot G \cdot (1 - v)}$$

$$\times \left[\frac{3 - 4v}{(r^2 + z^2)^{1/2}} + \frac{r^2}{(r^2 + z^2)^{3/2}} \right] dz. \qquad (36)$$

The shear strain is given by

$$d\epsilon_{rz} = \frac{1}{2} \left(\frac{\partial du_z}{\partial r} + \frac{\partial du_r}{\partial z} \right). \qquad (37)$$

The overall shear strain due to the distribution of Kelvinlets is then

$$\epsilon_{rz} = \int_0^{-\infty} d\epsilon_{rz} \qquad (38)$$

or, introducing equations (35)–(37) into equation (38) and rearranging

$$\epsilon_{rz} = -\frac{d \cdot \tau_c}{32 \cdot G \cdot (1-v)} \int_{-\infty}^0 \frac{z-s}{[r^2+(z-s)^2]^{5/2}}$$

$$\times [4v(z-s)^2 - 3(z-s) + (4v-3)r^2] ds. \qquad (39)$$

Solving equation (39) and introducing the result into

$$\tau_{rz} = 2 \cdot G \cdot \epsilon_{rz} \qquad (40)$$

yields the final result

$$\tau_{rz} = -\frac{3-4v}{16(1-v)} \tau_c \frac{d}{\sqrt{z^2+r^2}}. \qquad (41)$$

Equation (41) is the exact solution for the problem stated above, thus giving an upper bound for the shear stress induced by a fiber with residual stresses after dislocation punching, at a distance far enough from the end of the fiber for the corner singularity to be neglected and for the fiber to be satisfactorily approximated by a line of point forces. For a typical value of $v = 0.3$, the shear stress on the glide cylinder $r = d/2$ at a distance of one diameter away from the fiber end ($z = d$) is equal to $0.072\tau_c$, i.e. an order of magnitude less than the minimum stress necessary to move a dislocation in the lattice, if it is assumed that the critical interfacial shear stress τ_c is about equal to τ_f, the lattice friction stress. This leads to the conclusion that, apart from the stress induced by the singularity at the end of the fiber, the shear stress on the glide cylinder is negligible. Even if it is fully loaded through the interface, the fiber will have very little effect upon the loops punched at its ends. These will therefore be very close to the end of the fiber. We conclude that the length of the loop row as given by equation (28) is an adequate measure of the punching distance.

It is of interest to compare the above result to the similar situation of the backstress due to a sphere of radius r_s located at the origin of a cartesian coordinate system. The matrix shear stress on the glide cylinder of diameter $\sqrt{2}\, r$ due to a sphere subjected to an elastic hydrostatic strain ϵ is given by Johnson and Lee [23] as

$$\tau(\xi) = 96 \cdot \sqrt{2} \cdot G \cdot \beta' \cdot \epsilon \frac{\xi}{(2 \cdot \xi^2 + 1)^{5/2}} \qquad (42)$$

where $\xi = z/r_s$ and β' is a constant containing the matrix Poisson's ratio as well as the matrix and inclusion bulk moduli.

It is apparent that, as expected, the shear stress decays more rapidly than in the case of the cylinder. To allow a further quantitative comparison, we calcu-

late the stress on the glide cylinder when the residual stress in the sphere is such that the interfacial critical shear stress is reached at the intersection of the glide cylinder and the sphere. If the backstress due to the other loops is neglected, this is the maximal residual stress possible in the sphere since any higher stress would nucleate a loop at the interface. Introducing $\tau = \tau_f$ and $\xi = 1/\sqrt{2}$ into equation (42) gives a value for the maximum strain which, after introduction into equation (42), yields an equation for the shear stress on the glide cylinder

$$\tau^*(\xi) = 8\tau_f \frac{\xi}{(2 \cdot \xi^2 + 1)^{5/2}}. \qquad (43)$$

Choosing again a distance of one diameter away from the interface ($\xi = 3$) yields a value for τ^* equal to $0.015\tau_f$.

It can therefore be concluded that, in the case of the sphere as in the case of the cylinder, the backstress of the inclusion with a residual strain present after emission of loops is negligible at short distances away from the interface. This conclusion is supported by experimental observations of spherical and cylindrical inclusions [5] with the last punched loop located very close to the interface.

3. DISCUSSION

A parametric study was performed to investigate the influence of different variables on the number of punched loops n and the two critical length L_u and L_p. The system aluminium/alumina was chosen as an example, the properties of which are given in Table 1. Each of the parameters in Table 1 was varied while keeping all the other constant. It was found that only ΔT, L, d, τ_c and E_f had a significant influence on n, L_u or L_p. In particular, the volume fraction of fibers had a very small effect on these parameters. The length L_p as calculated from equation (9) was always small.

Figure 5(a–e) shows the effect of these parameters on the number of punched loops, using equation (23). Also shown in the same figure are the values predicted by the model of Ref. [10] which is briefly summarized in Appendix B.

Table 1. Thermal, mechanical and geometric parameters of the matrix and fibers used in the parametric study

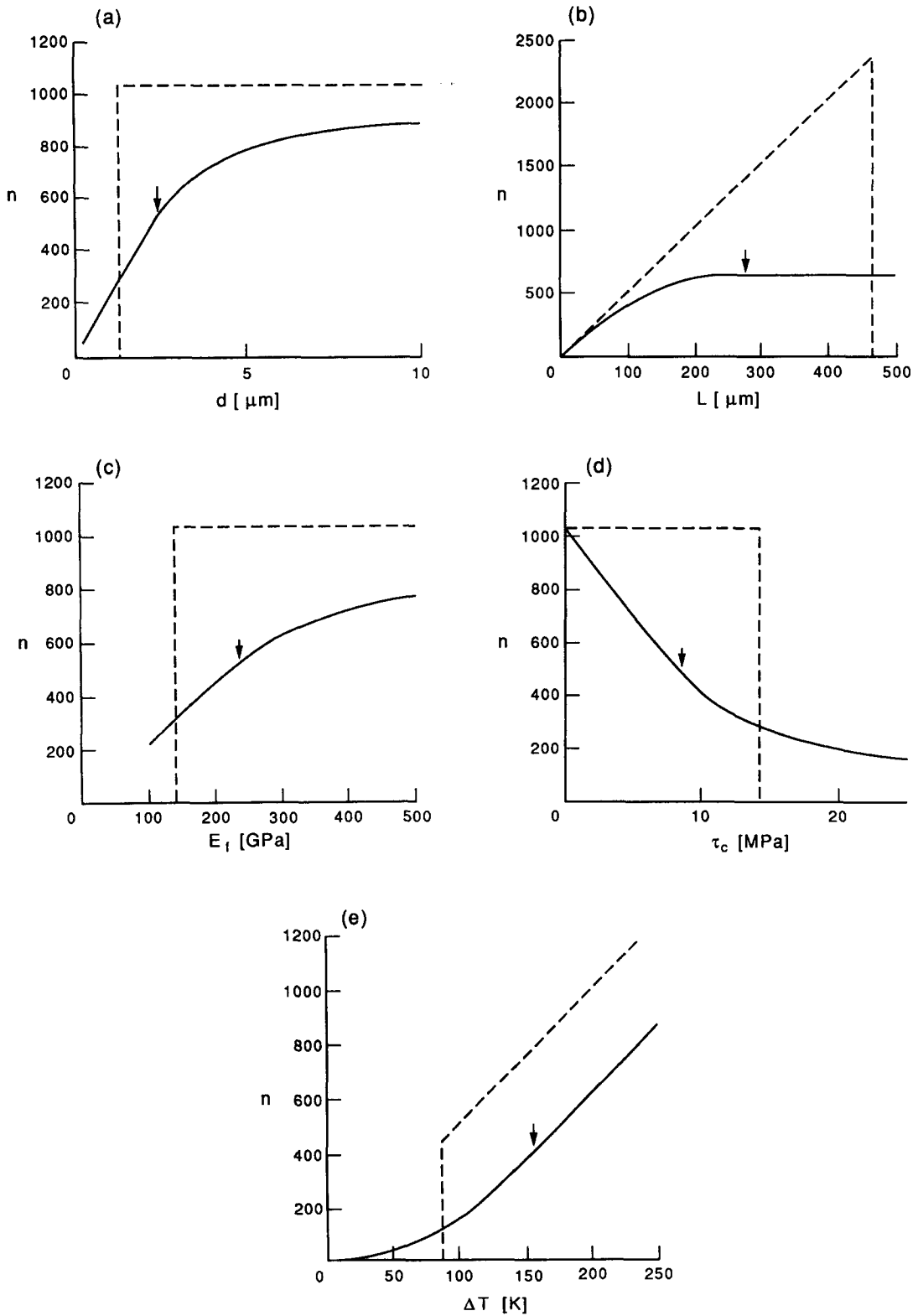| Parameter	Aluminium	Alumina
E (GPa)	72.5	300[a]
G (GPa)	30.1	—
v (—)	0.362	0.21
τ_c, τ_f (MPa)	5	—
α (10^6/K)	23.5	9[a]
b (nm)	0.286	—
L (µm)	—	200
d (µm)	—	3[a]
v_f (—)	—	0.1
σ_B (MPa)	—	0
ΔT (K)		200

[a]Saffimax™ values.

Fig. 5. (a) Number of loops punched as a function of the fiber diameter d, all other parameters in Table 1 being constant. (b) Number of loops punched as a function of the fiber length L, all other parameters in Table 1 being constant. (c) Number of loops punched as a function of the fiber elastic modulus E_f, all other parameters in Table 1 being constant. (d) Number of loops punched as a function of the matrix critical interfacial stress τ_c, all other parameters in Table 1 being constant. (e) Number of loops punched as a function of the temperature excursion ΔT, all other parameters in Table 1 being constant. Full curves: this model [equation (15)]. Dotted curves: model of Ref. [10] [equations (B1) and (B3)].

Equations (9) and (26) giving the two critical lengths L_p and L_u (wing $\sigma_B = 0$, see Appendix A) can be rewritten in dimensionless form

$$\frac{\beta \cdot L_p}{2} = \operatorname{arctgh}\left(\frac{\theta}{\Delta T}\right), \tag{44}$$

$$\frac{\beta \cdot L_u}{2} = \operatorname{arctgh}\left(\frac{\theta}{\Delta T}\right) + \sqrt{\left(\frac{\Delta T}{\theta}\right)^2 - 1} \tag{45}$$

where the intrinsic temperature θ is given by

$$\theta = \frac{4 \cdot \tau_c}{E_f \cdot \beta \cdot d \cdot \Delta \alpha} = \frac{\tau_c}{\Delta \alpha} \sqrt{\frac{2 \ln(v_f^{-1/2})}{G_m \cdot E_f}}. \tag{46}$$

Figure 6 shows a dimensionless plot of the critical lengths L_p and L_u as a function of the temperature interval ΔT, for all other parameters being constant [equations (44) and (45)]. The two curves delimit the three regions, elastic, elastic–plastic and elastic–plastic–unstrained. Similar projections can be done for the other variables defining L_p and L_u, introducing the appropriate intrinsic variables corresponding to θ.

It is apparent from Fig. 6 that, for $\Delta T > \theta$, a short fiber interface is completely elastic, a longer fiber interface is elastic–plastic while an even longer fiber interface is elastic–plastic–unstrained. For $\Delta T < \theta$ however, all fibers will have an entirely elastic interface. With the parameters chosen for the parametric study (Table 1), θ is equal to 7.8 K. It is also clear from Fig. 6 that there is a critical fiber length L^* (corresponding to the minimum of the L_u–ΔT curve), below which no temperature interval, however large, will produce an unstrained interfacial region

$$\frac{\beta \cdot L^*}{2} = \operatorname{arctgh}\left[\left(\frac{\sqrt{5}+1}{2}\right)^{-1/2}\right] + \left(\frac{\sqrt{5}-1}{2}\right)^{1/2}$$
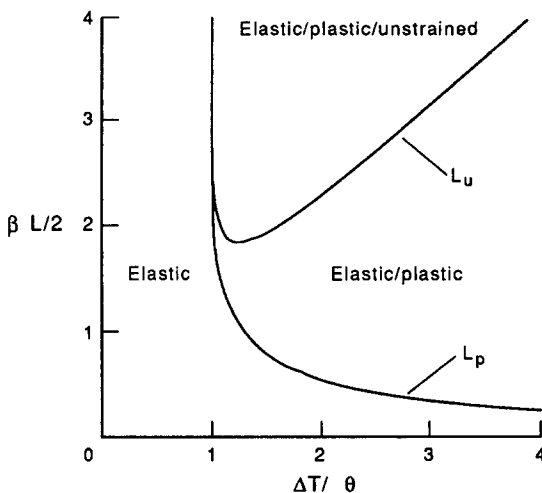
$$= 1.847. \tag{47}$$

Fig. 6. Dimensionless plot of the two critical lengths L_p and L_u as a function of the temperature excursion ΔT.

For the parameters in Table 1, L^* is equal to 19 μm.

The results above also show that the critical length L_p is small: for the parameters of Table 1, it is equal to 0.4 μm. In typical fiber reinforced metals subjected to large temperature variations, the prevailing regimes will thus be elastic–plastic or elastic–plastic–unstrained, i.e. relaxation by slip along part of the fiber will be observed. It follows that the first term in equation (26) can be neglected and since the third term is negligible (because σ_B is typically smaller than τ_c), equation (26) reduces to:

$$L_u \approx \frac{E_f \cdot d \cdot \Delta \alpha \cdot \Delta T}{2 \cdot \tau_c}. \tag{48}$$

The boundary between the elastic–plastic regime and the elastic–plastic–unstrained regime is marked by an arrow in Fig. 5(a–e). For small values of L, τ_c and ΔT, and large values of E_f and d, the value of n calculated from equation (23) tends toward that predicted by equation (B3) which represents an upper bound value; as expected, this value is never exceeded. An important qualitative and quantitative discrepancy is observed between our model and that of Ref. [10], since equation (23) does not predict a set of critical parameters for which punching is suppressed (except when the interface is completely elastic for $L = L_p$, at which point punching has not yet been activated).

A possible reason why punching suppression is predicted by the model of Ref. [10] is its implicit assumption that the loops are punched *all at once* rather than one after the other. As the number of loops to be simultaneously punched increases, so does the total energy needed for punching. This energy may therefore exceed that released during the relaxation of the spheroid, which would suppress punching. A second possible reason is that, with the geometry assumed in Ref. [10], dislocations are emitted along the side of the fiber, and therefore must travel a distance proportional to the fiber length if L_r, defined as the distance between the leading loop of the row and the fiber tip, remains constant. This renders the energy dissipated by motion of the dislocation loops proportional to L when L_r and d remain constant [see equation (15) of Ref. [10], reproduced here in Appendix B as equation (B2)]. In the analysis presented here, loops are punched sequentially rather than simultaneously, and are all emitted at the fiber end. We therefore reach the conclusion that no fiber is too long to punch loops. Rather, long fibers reach a critical length L_u, above which *subsequent* punching is inhibited [Fig. 5(b)].

The assumption in Ref. [10] that all dislocation loops are emitted simultaneously is relaxed in a modified version of that model to be published elsewhere [26]. We find that loop punching is still suppressed for long fibers. This indicates that the second explanation proposed above, namely the

difference in inclusion geometry and dislocation emission sites, is at the root of the discrepancy between model in Refs [10, 26] and that presented here. For cylindrical fibers, we believe the present model is more appropriate, whereas that of Refs [10, 26] is better for rounded inclusions which are more realistically modelled as a spheroid.

4. CONCLUSIONS

The shear lag model by Cox [13] can be adapted to predict thermal mismatch stresses between an elastic fiber and a matrix capable of slip, including the case where part of the fiber–matrix interface is plastic and prismatic loops are punched at the fiber end. The number of loops reaches a maximum value when the fiber central portion is strained by interfacial stresses to the point where it shows no mismatch with the matrix.

The effect of the fiber residual stress field on the loops is examined away from the corner singularity and found to be small, thus allowing to use existing expressions [18] to determine the punching distance (and thus the dislocation density on the glide cylinder) from the total number of punched loops.

A parametric study is performed on the system aluminium–alumina and the results for the total number of loops punched are compared to those predicted by the model of Ref. [10]. A discrepancy between the two models is found which is due to the different geometric and physical assumptions used.

An additional proof is given for the backstress exerted by a row of loops at equilibrium on its source. The backstress is small even for a large number of loops and is thus neglected for the parametric study.

REFERENCES

1. G. C. Weatherly, *Metals Sci. J.* **2**, 237 (1968).
2. E. Votava, *Acta metall.* **11**, 1105 (1963).
3. W. Carrington, K. F. Hale and D. McLean, *Proc. R. Soc.* A259, 203 (1961).
4. D. A. Jones and J. W. Mitchell, *Phil. Mag.* **3**, 1 (1958).
5. D. C. Dunand and A. Mortensen, *Acta metall. mater.* **39**, 127 (1991).
6. D. C. Dunand and A. Mortensen, *Mater. Sci. Engng A.* In press.
7. C. B. Childs and L. M. Slifkin, *Br. J. appl. Phys.* **16**, 771 (1965).
8. C. T. Kim, J. K. Lee and M. R. Plichta, *Metall. Trans.* **21A**, 673 (1990).
9. M. Vogelsang, R. J. Arsenault and R. M. Fisher, *Metall. Trans.* **17A**, 379 (1986).
10. M. Taya and T. Mori, *Acta metall.* **35**, 155 (1987).
11. T. Christman and S. Suresh, *Acta metall.* **36**, 1691 (1988).
12. J. D. Eshelby, *Proc. R. Soc.* A241, 376 (1957).
13. H. L. Cox, *Br. J. appl. Phys.* **3**, 72 (1952).
14. A. Kelly and N. H. Macmillan, *Strong Solids*, p. 264. Oxford Science Publ. (1986).
15. N. F. Dow, *General Electric Report R. 63SD61* (1963). Reported by Kelly and Macmillan [14].
16. D. M. Schuster and E. Scala, *Trans. metall. Soc. A.I.M.E.* **230**, 1635 (1964).
17. W. R. Tyson and G. J. Davies, *Br. J. appl. Phys.* **16**, 199 (1965).
18. D. C. Dunand and A. Mortensen, *Scripta metall. mater.* **25**, 607 (1991).
19. G. J. Schneider and H. D. Conway, *J. comp. Mater.* **3**, 116 (1969).
20. C. Atkinson, J. Avila, E. Betz and R. E. Smelser, *J. Mech. Phys. Solids* **30**, 97 (1982).
21. N. Phan Thien, *Fibre Sci. Tech.* **12**, 235 (1979).
22. L. D. Landau and E. M. Lifshitz, *Theory of Elasticity*, p. 29. Pergamon Press, Oxford (1959).
23. W. C. Johnson and K. C. Lee, *Acta metall.* **31**, 1033 (1983).
24. D. Hull, *Introduction to Dislocations*, 2nd edn, p. 208. Pergamon Press, Oxford (1975).
25. K. Tanaka and T. Mori, *J. Elasticity* **2**, 199 (1972).
26. D. C. Dunand and A. Mortensen, *Scripta metall. mater.* In press.

APPENDIX A

Loop Backstress on the Fiber

Using a virtual work argument, we derived in a previous publication [18] the backstress σ_B on an inclusion by a row of n loops in a crystal with friction stress τ_f

$$\sigma_B = \frac{4n\tau_f b}{d}. \tag{A1}$$

In what follows, we present an alternate proof for this result. Consider a hypothetical crystal with zero friction stress containing the same inclusion which has punched the same row of n coaxial, circular, prismatic loops of length l and Burgers vector b. If the loops were free to move, they would repel each other and glide an infinite distance away from the inclusion, since there would be no friction stress to stop them. Imagine now that the hypothetical crystal is subjected to an external shear stress τ which prevent the loops from escaping to infinity. If the loops are assimilated to straight edge dislocations of the same length, the force F on the inclusion by the pile-up is [24]

$$F = n\tau bl. \tag{A2}$$

If the value of this external shear stress is chosen as that of the friction stress of the real lattice τ_f, the spacing of the loops and therefore the backforce F_B on the inclusion is the same in both cases

$$F_B = n\tau_f bl. \tag{A3}$$

The real crystal with a friction stress τ_f has thus been replaced by an hypothetical crystal with zero friction stress but an external shear stress τ_f. Since the spacings of the loop are the only parameters determining the magnitude of the backforce, it is identical in both situations. Assuming that the loops of length $l = \pi d$ exert a force $F_B = \sigma_B \pi d^2/4$ at the end of the fiber of same diameter, the results given in equation (A1) is found by introducing the two values above in equation (A3).

Equation (A1) can then be introduced in equation (26) as well as equation (21), leading to equation (22). It appears from inspection that, even for large values of n, the terms containing σ_B are small compared to the other terms in these

equations. The backstress of the loops on the fiber has thus a minor effect on the stress-state of the fiber and the interface.

In equation (16), the backstress is added as a constant to the longitudinal stress of the fiber; this in an approximation since the backstress is not due to a localized force at the end of the fiber but rather to the stress field of the row of loops that is applied along the whole length of the fiber. Since this field decays rapidly with distance and since the backstress is of small magnitiude, this approximation is inconsequential.

APPENDIX B

Summary of Taya and Mori's Model [10]

This model predicts the number of loops and the punching distance L_r for a misfitting fiber which is assimilated to a prolate spheroid of major axis L and minor axis d. Due to thermal mismatch, the fiber punches loops, thus forming a plastic zone modelled as another prolate spheroid of same minor axis as the fiber and major axis $L + 2L_r$. The punching distance is determined by solving

$$\frac{d(U + W)}{dL_r} = 0 \tag{B1}$$

where W is the work done by the motion of the dislocation loops against the lattice friction stress τ_f [25]

$$W = \frac{\pi}{3} L_r L d \Delta\alpha \Delta T \tau_f. \tag{B2}$$

$\Delta\alpha$ is the CTE difference between fiber and matrix and ΔT is the temperature excursion of the composite. The potential energy U is calculated using Eshelby's equivalent inclusion method [12] and is of the form $U(L, L_r, d, \Delta\alpha, \Delta T, G_m, G_f, \lambda_m, \lambda_f, \nu_m)$, where G, λ and ν are shear modulus, Lamé constant and Poisson's ratio, and the subscripts f and m denote fiber and matrix respectively.

A noteworthy feature of this model is that each parameter in equation (B1) has a critical value for which the punching distance becomes zero, separating a regime of positive and negative punching distances. The model of Ref. [10] predicts that punching is suppressed in the latter regime and this result is justified by showing that the energy needed to move the dislocations against the lattice friction stress is larger than the elastic energy released by relaxation. This leads to the unexpected result that the punching length decreases and finally becomes zero as the fiber length (and thus the total mismatch) increases. In the regime where loops are emitted, they assume that n_{max} loops are emitted at each end, corresponding to the total relaxation of the longitudinal mismatch strain

$$n_{max} = \frac{\Delta\alpha \Delta T L}{2b}. \tag{B3}$$

Figure 5(a–e) shows this value as dotted lines which drop to zero at a critical value corresponding to the onset of negative punching distance regime predicted by numerically solving equation (B1) for $L_r = 0$. We relax this last assumption in a forthcoming publication [26], and reach the conclusion that beyond a certain fiber length, punching suppression is nonetheless predicted, in contradiction with the model presented in the body of this article.

APPENDIX C

Nomenclature

b = Burger's vector
d = fiber diameter
e = uniaxial strain
E = elastic modulus
F = force
F_B = backforce
G = shear modulus
H = function
H'' = constant used in equation (1)
l = dislocation length
L = fiber length at low temperature inside the matrix
L_f = fiber length at low temperature outside the matrix
L_m = matrix hole length at low temperature without fiber
L_o = fiber length at high temperature
L_p = fiber critical length (elastic–plastic interface)
L_r = loop row length
L_u = fiber critical length (elastic–plastic–unstrained interface)
L^* = fiber length below which the fiber is never unstrained
n = loop number (approximate solution)
n' = loop number (exact solution)
p = fiber load
r_s = sphere radius
u = displacement
v = parameter defined in equation (27)
v_f = fiber volume fraction
w = displacement
x = coordinate
z = coordinate

Subscripts

    f = fiber
    m = matrix
r, z, θ = coordinate
    i = 1, 2, 3
    max = maximal

Greek symbols

α = coefficient of thermal expansion
β = parameter defined in equation (4)
β' = parameter used in equation (42)
δ_{ij} = Kronecker symbol
$\Delta\alpha$ = CTE difference between matrix and fiber
ΔT = temperature difference
ϵ = shear strain
θ = critical value of ΔT
λ = Lame's constant
ν = Poisson's ratio
ρ = dislocation density
σ = fiber longitudinal stress
$\bar{\sigma}$ = average stress
σ_B = backstress
σ_e = elastic contribution to fiber stress
σ^* = fiber stress at L_p
τ = interfacial shear stress
τ_c = critical interfacial shear stress
τ_f = lattice friction stress
τ^* = shear stress on glide cylinder
ξ = dimensionless coordinate
ζ = dimensionless coordinate